ACS APPLIED MATERIALS & INTERFACES

RESEARCH ARTICLE

www.acsami.org

Evolved Phase Separation toward Balanced Charge Transport and High Efficiency in Polymer Solar Cells

Haijun Fan,[†,‡] Maojie Zhang,[†,‡] Xia Guo,[†,‡] Yongfang Li,[†,*] and Xiaowei Zhan[*,†]

[†]Beijing National Laboratory for Molecular Sciences, CAS Key Laboratory of Organic Solids, Institute of Chemistry, Chinese Academy of Sciences, Beijing 100190, China

[‡]Graduate University, Chinese Academy of Sciences, Beijing 100049, China

ABSTRACT:

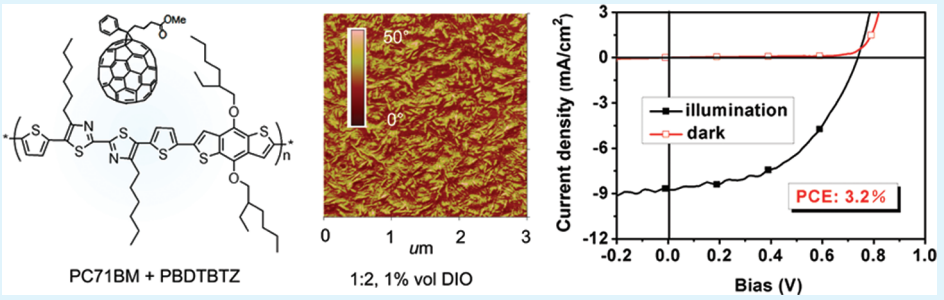

Understanding effect of morphology on charge carrier transport within polymer/fullerene bulk heterojunction is necessary to develop high-performance polymer solar cells. In this work, we synthesized a new benzodithiophene-based polymer with good self-organization behavior as well as favorable morphology evolution of its blend films with $PC_{71}BM$ under improved processing conditions. Charge carrier transport behavior of blend films was characterized by space charge limited current method. Evolved blend film morphology by controlling blend composition and additive content gradually reaches an optimized state, featured with nanoscale fibrilla polymer phase in moderate size and balanced mobility ratio close to 1:1 for hole and electron. This optimized morphology toward more balanced charge carrier transport accounts for the best power conversion efficiency of 3.2%, measured under simulated AM 1.5 solar irradiation 100 mW/cm^2, through enhancing short circuit current and reducing geminate recombination loss.

KEYWORDS: polymer solar cell, morphology, charge transport, conjugated polymer, additive, phase separation

INTRODUCTION

Polymer/fullerene blend solar cells, the largest and most important division of solution-processed organic solar cells, have gained much attention during the past few years for their potential for achieving large area, flexible photovoltaic devices through low-cost solution-processing techniques.[1−3] Encouraging achievements have been obtained in virtue of the rational molecule design developed in these two years, yielding amazing power conversion efficiencies (PCEs) around 7−8%.[4,5] As one of the photovoltaic technologies leading the development of next generation on low-cost power production, polymer/fullerene solar cells with PCEs of ∼10% would be convictive to be considered in widespread applications.[6] Toward this target, not only endeavors on designing novel materials with strong absorption, high hole mobility, and suitable energy levels should be encouraged,[7−9] but also the in-depth understanding of the physical process happened in real devices are highly needed, which would contribute much to make clear the potential of different polymer/fullerene solar cells and ultimately optimize the device performances.[10,11] Although skillful methods aiming at optimizing active layers, the most important components in photovoltaic devices where essential photoelectric conversion process takes place, have been successfully explored, such by introducing processing additives,[12] annealing in solvent or thermally,[13,14] adopting cosolvents or orthogonal solvents,[15,16] research on probing morphology transformation of active layers and thus resulted charger transport and photovoltaic performance varied with processing methods changing is still a fascinating subject and worthy of being studied further.[17,18]

Morphology has been considered to be the critical factor influencing the performance improvement of polymer/fullerene solar cells, by affecting exciton generation and transfer, dissociation and charge separation, charge transport and collection at separated electrodes.[19,20] Since the introduction of bulk heterojunction (BHJ) architecture in polymer/fullerene solar cells,[21] the interface area could be enhanced enormously by forming active layers consisting of interpenetrating blends of donor and acceptor components. Thus, exciton dissociation and charge

Received: June 29, 2011
Accepted: August 4, 2011
Published: August 04, 2011

Scheme 1. Synthesis of Polymer PBDTBTZ

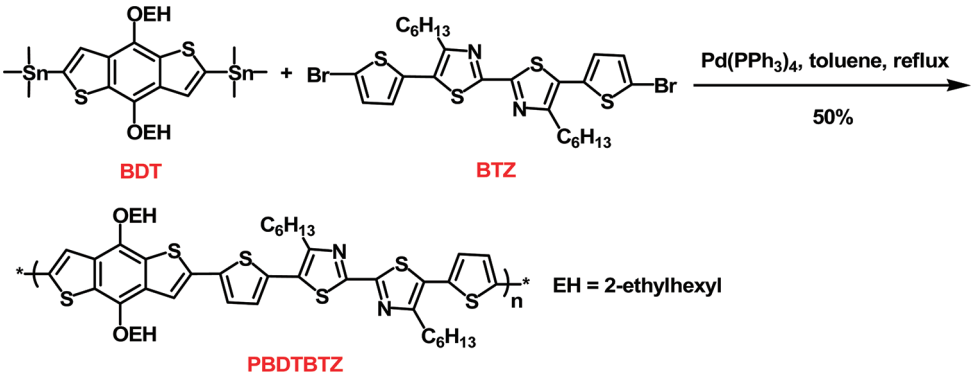

separation are also facilitated.[4] Nevertheless, challenges still exist in maximizing the interfaces while preserving the moderate scale phase separation within exciton diffusion range, normally 10 nm, together with the continuous percolated networks for charge carrier transport.[22] Recently, polymers with mesoscopic order or crystalline are widely developed for their unique self-organization behavior.[17,23,24] Improved charge carrier transport thus can be achieved, which is of vital importance, especially for hole transport in polymer/fullerene BHJ solar cells. It is the hole transport that dominates the competition with back recombination due to the less mobility of holes in polymer than that of electrons in fullerene.[25,26] Thus, better hole mobility often means higher device performance. However, usual methods adopted to modify the nanoscale phase separation morphology often produce excess phase separation on both the meso- (>100 nm) and nanoscales (<20 nm),[27] and large domains with sizes larger than recommended 10 nm have been observed.[28,29] Also, isolated domains, ruining the interpenetrating networks and hindering the direct path for electrons and holes to travel toward the electrodes, are hardly avoided.[30] These render us to consider the balance between phase separation and charge transport.

In a previous communication, we reported that a new benzodithiophene-bithiazole copolymer exhibited good photovoltaic performance in combination with $PC_{71}BM$.[31] Here, we report a related benzodithiophene-bithiazole copolymer with good self-organization behavior for BHJ solar cells. We focus on the relationship between morphology and device performance. Evolved morphology of the donor/acceptor blend films was achieved through optimizing blend composition and additive content. The evolved morphology accounts for the PCE improvement from 2.2 to 3.2%. The effects of evolved phase separation on charge transport and efficiency in the solar cells are investigated.

EXPERIMENTAL SECTION

Measurement. The ^{1}H NMR spectra were recorded on a Bruker DMX-400 spectrometer, $CDCl_3$ as the solvent. Chemical shifts in the NMR spectra were reported in ppm relative to the singlet at 7.26 ppm for $CDCl_3$. The molecular weight of the polymer was measured by gel permeation chromatography (GPC) using polystyrene standards as calibrants. The thermogravimetric analysis (TGA) measurement was performed using Perkin-Elmer TGA-7 under N_2 at a heating rate of 10 °C min^{-1}. The UV−vis spectra were recorded by Hitachi U-3010 spectrometer. The cyclic voltammetry was performed on a Zahner IM6e electrochemical workstation with a three-electrode system in 0.1 M tetrabutylammonium hexafluorophosphate (Bu_4NPF_6) acetonitrile solution at a scan rate of 100 mV s^{-1}. In this system, Pt plate dip-coated with polymer films was adopted as the working electrode, while Pt wire was used as the counter electrode. The reference electrode was Ag/Ag^+ electrode (0.01 M $AgNO_3$, 0.09 M Bu_4NPF_6 in acetonitrile). For photovoltaic devices, the current−voltage ($J-V$) characteristic measurement was performed in glovebox under simulated AM 1.5 irradiation (100 mW cm^{-2}) via a computer-controlled Keithley 236 source measure unit combined with an Oriel 96000 150 W solar simulator. The thickness of active layers was determined by an Ambios Technology XP-2 profilometer. The external quantum efficiency (EQE) of devices was measured using a lock-in amplifier (SR830, Standford Research Systems) coupled with a WDG3 monochromator and a 500 W xenon lamp, light intensity calibrated with a standard silicon photovoltaic cell. Atomic force microscopy (AFM, NanoMan VS, Veeco, USA) and transmission electron microscopy (TEM, JEM-1011, JEOL, Japan) were manipulated to characterize the morphology of blend films.

Synthesis. The route for polymer synthesis is presented in Scheme 1, in which monomers 2,7-bis(trimethyltin)-4,5-bis(2-ethylhexyloxy)benzo[2,1-b:4,5-b′]dithiophene (BDT)[32,33] and 5,5′-bis(2-bromo-thiophene-5-yl)-4,4′-dihexyl-2,2′-bithiazole (BTZ)[34] were synthesized according to the reported procedures.

Poly[4,5-bis(2-ethylhexyloxy)benzo[2,1-b:4,5-b′]dithiophene-2,7-diyl-alt-5,5′-dithienyl-4,4′-dihexyl-2,2′-bithiazole-2,2′-diyl] (PBDTBTZ). Monomer 5,5′-bis(2-bromo-thiophene-5-yl)-4,4′-dihexyl-2,2′-bithiazole (656 mg, 1 mmol), 2,7-bis(trimethyltin)-4,5-bis(2-ethylhexyloxy)benzo[2,1-b:4,5-b′]dithiophene (742 mg, 1 mmol), and 25 mL of dry toluene were added into a 50 mL two-necked round-bottom flask. After a 20 min deoxygenation process with N_2, 25 mg (22 μmol) $Pd(PPh_3)_4$ was added. Keep flushing with N_2 for 20 min, and then the mixture was heated to reflux for 12 h. After the mixture was cooled down to room temperature, 200 mL of methanol was poured into the flask. The solid was filtered through a Soxhlet thimble, and was extracted with methanol, hexane, and chloroform subsequently. The product was further purified by column chromatography on silica gel, chloroform as the eluent. After further concentration and reprecipitation with methanol, final polymer was collected and dried under vacuum overnight. Yield: 477 mg (50%). ^{1}H NMR ($CDCl_3$, 400 MHz), δ (ppm): 7.41−7.11 (br, 6H), 4.14 (br, 4H), 2.91 (br, 4H), 1.85−1.34 (br, 34H), 0.88−0.79 (br, 18H).

Fabrication of Photovoltaic Devices. Polymer/fullerene BHJ solar cells were fabricated with a structure of ITO/PEDOT:PSS/PBDTBTZ:$PC_{71}BM$/Ca/Al. Prior to device fabrication, patterned indium tin oxide (ITO) glass (1.5 cm × 1.5 cm, sheet resistance, 30 Ω □$^{-1}$) was cleaned in an ultrasonic bath of detergent, deionized water, acetone and isopropanol. After being treated in an ultraviolet-ozone chamber (Jelight Company, USA) for 20 min, the precleaned ITO glass was spin-coated a ~30 nm thick poly(3,4-ethylenedioxythiophene):poly(styrene

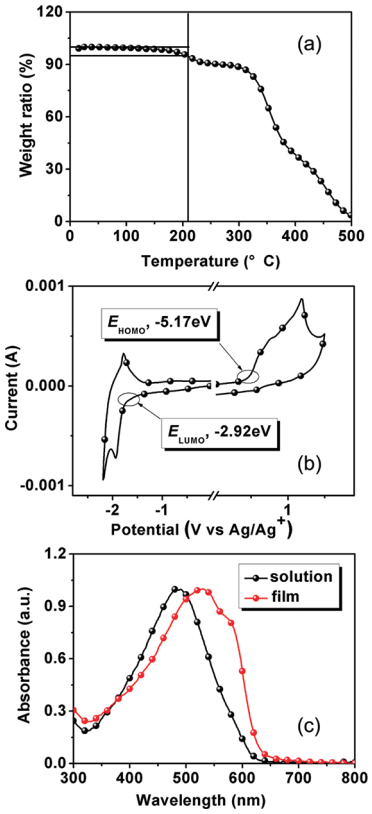

Figure 1. (a) TGA, (b) CV, (c) UV−vis absorption curves of polymer PBDTBTZ.

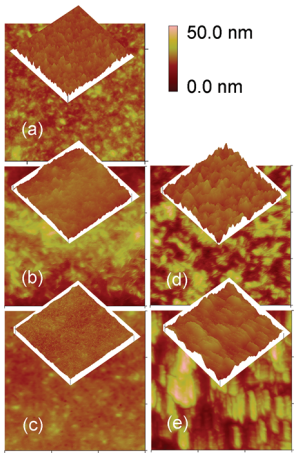

Figure 2. Tapping-mode AFM height images (3 μm × 3 μm) of PBDTBTZ:$PC_{71}BM$ blend films drop-cast from dichlorobenzene solutions with (a) 1:1 weight ratio, (b) 1:2 weight ratio, (c) 1:3 weight ratio, (d) 1:2 weight ratio containing 1% DIO, (e) 1:2 weight ratio containing 2% DIO. The insets cover exactly the same regions with the variations in height shown explicitly.

sulfonate) (PEDOT:PSS, Baytron P VP AI 4083, Germany) film and was baked at 150 °C for 30 min. Then, active layers were drop-cast onto the surface of PEDOT:PSS from the dichlorobenzene (DCB) solution of PBDTBTZ/$PC_{71}BM$ blend. Finally, layers of calcium (Ca, ~20 nm) and aluminum (Al, ~50 nm) were thermally evaporated under a vacuum (1×10^{-4} Pa) through a shadow mask. The active area of the device was 4 mm^2. In addition, to determine the charge carrier mobility, hole-only and electron-only devices were also fabricated. For hole-only devices, an Au layer (40 nm) was used as top electrode for its higher work function (Φ, 5.0 eV). The large energy barrier ($\Delta E \approx 1.3$ eV) between Au work function and LUMO level of $PC_{71}BM$ would suppress the electron injection from the top electrode, and thus render the devices hole-only characteristic. For electron-only devices, the PEDOT:PSS layer was replaced with Al for its relatively lower work function. The hole injection into PBDTBTZ thus could be suppressed. Meanwhile, to facilitate the electron injection from $PC_{71}BM$ to the top electrode by forming Ohmic contacts, 50 nm Al was evaporated as the top electrode. Thus, electron-only devices with Al/PBDTBTZ:$PC_{71}BM$/Al structure were fabricated.

RESULTS AND DISCUSSION

Synthesis and Characterization of Polymer. PBDTBTZ was synthesized by Stille coupling copolymerization reaction between 2,7-bis(trimethyltin)-4,5-bis(2-ethylhexyloxy)benzo-[2,1-b:4,5-b′] dithiophene and 5,5′-bis(2-bromo-thiophene-5-yl)-4,4′-dihexyl-2,2′-bithiazole using $Pd(PPh_3)_4$ as the catalyst (see Scheme 1). The polymer shows good solubility in common organic solvents such as chloroform, toluene, chlorobenzene, and dichlorobenzene. The weight average molecular weight (M_w) and a polydispersity index of PBDTBTZ was estimated by GPC to be 5200 and 1.67, respectively. TGA analysis reveals a 5% weight loss appearing at 210 °C, implying enough thermal stability of the polymer for photovoltaic application (Figure 1a).

The cyclic voltammogram of the polymer is presented in Figure 1b. Estimated from the onset oxidation potential (E_{ox}) and reduction potential (E_{red}), the highest occupied molecular orbital energy level (E_{HOMO}) and the lowest unoccupied molecular orbital energy level (E_{LUMO}) as well as the energy gap (E_g) of the polymer were determined to be −5.17, −2.92, and 2.25 eV, respectively, according to the equation $E_{HOMO} = -e(E_{ox} + 4.71)$ (eV), $E_{LUMO} = -e(E_{red} + 4.71)$ (eV), and $E_g = E_{LUMO} - E_{HOMO}$ (eV).[34] The relatively deep HOMO level endows the polymer with good air stability as well as the potential to achieve high open-circuit voltage (V_{oc}) in BHJ solar cells. Moreover, the LUMO gap between PBDTBTZ and $PC_{71}BM$ is about 0.98 eV, which is large enough to provide a downhill driving force for the ultrafast photoinduced electron transfer.

Remarkable red-shift (~50 nm) of absorption maximum in film state relative to that in solution state has been observed (Figure 1c), indicating strong intermolecular interaction. Additionally, pronounced vibronic shoulder at 590 nm implies the ordered arrangement in film due to strong $\pi-\pi$ stacking between PBDTBTZ backbones, a typical feature similar to that of regioregular poly(3-hexylthiophene) (P3HT).[35]

Morphology Evolution of PBDTBTZ/$PC_{71}BM$ Blend Films. In a BHJ photovoltaic device, the active layer is typically the composite of a polymer donor and a soluble fullerene acceptor, codeposited from solution. The morphology of blend films, especially the size and purity of segregated domains, is a function of the self-organizing tendencies of the donor and acceptor components, the interaction between them and the process parameters. Any process parameter such as solvent, evaporating rate, blend composition and thermal treatment could affect the morphology of blend films. Due to the difference in structure, polymers present different features such as mixing entropy, equilibrium configuration, nucleation, and crystallization. Methods used to optimize the morphology of one polymer may not be applicable for another one. We have examined the effects of thermal annealing and solvent annealing for PBDTBTZ, but none of them exhibited positive effects. Thus, two other ways,

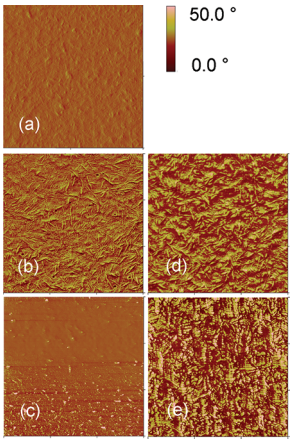

Figure 3. Tapping-mode AFM phase images (3 μm × 3 μm) of PBDTBTZ:$PC_{71}BM$ blend films drop-cast from dichlorobenzene solutions with (a) 1:1 weight ratio, (b) 1:2 weight ratio, (c) 1:3 weight ratio, (d) 1:2 weight ratio containing 1% DIO, (e) 1:2 weight ratio containing 2% DIO.

namely by optimizing blend composition and additive content, were tried.

We explored the effect of blend composition by altering donor/acceptor weight ratio first. Figure 2 shows the AFM height images of PBDTBTZ:$PC_{71}BM$ blend films drop-cast from different solutions. An adoptable weight ratio between PBDTBTZ and $PC_{71}BM$ was determined to be 1:2, based on its coarser surface since considerably coarse surface could lead to high efficiency of polymer/fullerene solar cells.[36,37] The 1:2 film has a 2.76 nm root-mean-square roughness (R_{rms}), larger than that for 1:1 or 1:3 films (R_{rms}, 2.49 and 1.79 nm, respectively). Subsequently, 1 and 2% (volume) 1,8-diiodooctane (DIO) were added into the solution with 1:2 weight ratios to further adjust film morphology. Also, coarser surfaces with larger domains were observed with increasing DIO content. Films with added 1 and 2% DIO give R_{rms} of 6.94 and 7.34 nm, respectively, both larger than that of film without additive (1:2, R_{rms}, 2.76 nm). It is reasonable for that the aggregation and order of fullerene could be enhanced through a gradual evaporation of host solvent by DIO addition,[27] because of the selective dissolvability of fullerene in additive as well as the higher boiling point of additive than host solvent.[38] However, the film morphology by 2% DIO addition is thought to be excessively aggregated, displaying large domains exceeding 1 μm in length, which would disfavor the charge transport and lower the device performance.

More detailed information on phase separation could be obtained by AFM phase images. Obvious phase contrast was observed, shown in Figure 3. With increasing donor/acceptor ratio or additive content, nanoscale phase separation can be enhanced. Relatively smooth phase without obvious phase separation was observed for 1:1 blend ratio (Figure 3a). At 1:2 blend ratio, the phase consisting of ~200 nm long fibrils with an aspect ratio ~8 was observed (Figure 3b). At 1:3 ratio relatively smooth phase with scattered spots was observed (Figure 3c). Adding 1% DIO into 1:2 blend makes fibril phase broadening, giving ~4 mean aspect ratio (Figure 3d). Adding 2% DIO into 1:2 blend makes fibril phase further broadening to form grains (Figure 3e).

The X-ray diffraction patterns of pure PBDTBTZ and PBDTBTZ:$PC_{71}BM$ (1:2, w/w) blend are shown in panels a and b in Figure 4. In Figure 4a, sharp peak at $2\theta = 5.7°$ and broad

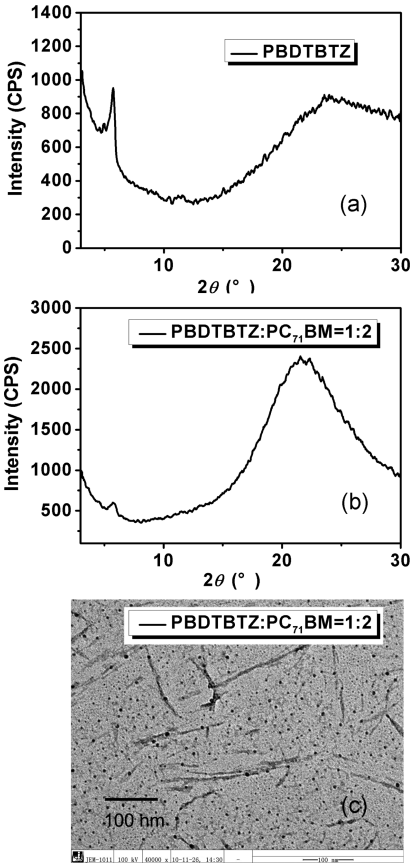

Figure 4. (a) XRD patterns of pristine PBDTBTZ, (b) PBDTBTZ:$PC_{71}BM$ (1:2, w/w) blend, and (c) TEM image of PBDTBTZ:$PC_{71}BM$ (1:2, w/w) blend.

peak around $2\theta = 24°$ confirm the existence of polymer crystals in pristine PBDTBTZ film. Their d values, 1.54 and 0.38 nm, correspond to the intermolecular lamellar spacing and $\pi-\pi$ stacking distance in polymer crystals, respectively, which is similar to that of the reported polymer containing similar backbone structure.[31] In blend film, distinct X-ray diffraction peaks can also be observed, appearing at different angles with different d values. As shown in Figure 4b, small peak appearing at $2\theta = 5.9°$ with a d value of 1.50 nm, similar to that in pristine PBDTBTZ film, suggests the formation of polymer crystals, while the broad and strong peak around $2\theta = 21°$ could be assigned to the diffraction peak of fullerene, indicating probable existence of ordered fullerene aggregates.[39] In TEM image of PBDTBTZ:$PC_{71}BM$ (1:2, w/w) blend (Figure 4c), ~200 nm polymer nanowires and nanoscale fullerene aggregates could also be observed, in coincidence with the analysis discussed above. These ordered polymer crystals and fullerene aggregates may change with processing condition varied, and exhibit complex influence on device performance.

Photovoltaic Properties. The evolved morphology of PBDTBTZ:$PC_{71}BM$ blend films through optimizing blend ratios and additive contents exhibits significant impacts on their photovoltaic properties. Typical current density−voltage ($J-V$) curves and corresponding external quantum efficiencies (EQEs) are presented in Figure 5, whereas detailed photovoltaic data, collected from more than 40 individual devices and given by statistical average, are listed in Table 1. With donor/acceptor ratio

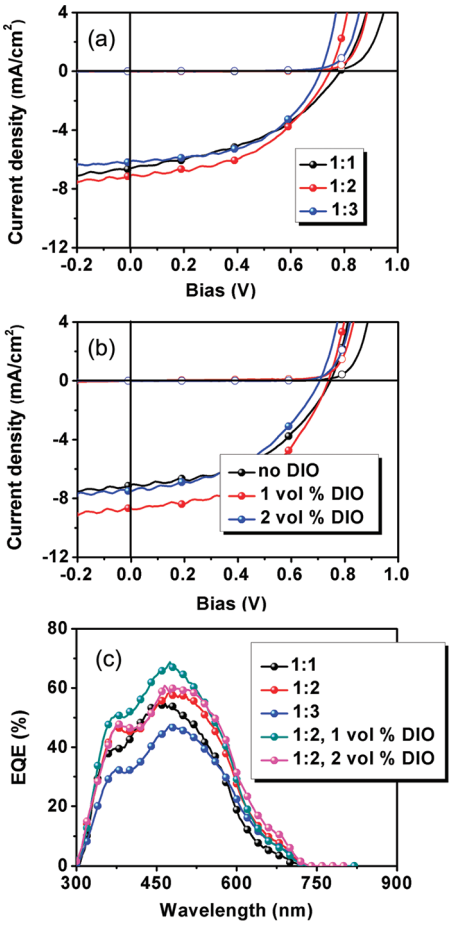

Figure 5. Current density−voltage ($J-V$) curves of photovoltaic devices achieved by altering (a) blend ratios and (b) additive contents, as well as (c) EQE curves.

Table 1. Photovoltaic Properties of BHJ Solar Cells Based on PBDTBTZ:$PC_{71}BM$

device condition	V_{oc} (V)	J_{sc} (mA/cm^2)	FF	PCE (%)
1:1	0.790	6.61	0.424	2.21
1:2	0.750	7.06	0.482	2.55
1:3	0.710	6.11	0.530	2.30
1:2, 1% DIO	0.740	8.71	0.496	3.20
1:2, 2% DIO	0.710	7.51	0.450	2.40

increasing, devices exhibit slight decrease in open-circuit voltage (V_{oc}), increase in fill factor (FF), and peak values of short-circuit current (J_{sc}) and PCE at 1:2 ratio. The highest PCE at 1:2 ratio is attributed to the evolved morphology which exhibits the largest R_{rms} and continuous fibrillar phase.

With additive content increasing, devices exhibit slight decrease in V_{oc} and peak values of J_{sc}, FF and PCE at 1% DIO. The best performance at 1% DIO is ascribed to the optimized morphology. The drop in V_{oc}, FF an,d PCE caused by adding 2% DIO could be attributed to large size phase separation.

Generation of Photocurrent. Improved J_{sc} accompanied with optimized morphology can be further understood from the process of photocurrent generation. To get large photocurrent, strong and broad absorption of the active layer is required.

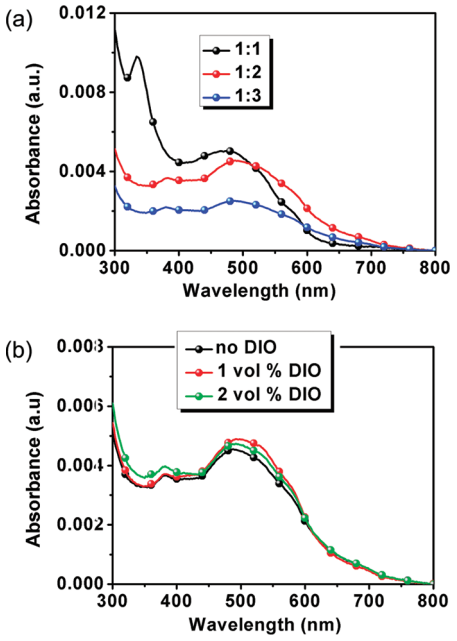

Figure 6. UV−vis absorption of PBDTBTZ:$PC_{71}BM$ blend films formed under (a) different PBDTBTZ/$PC_{71}BM$ weight ratios and (b) different additive contents with PBDTBTZ/$PC_{71}BM$ weight ratio of 1:2.

UV−vis absorption spectra for unit thickness of PBDTBTZ:$PC_{71}BM$ blend films formed under different conditions are shown in Figure 6. All films are formed under the same conditions as device fabricated. The absorption peaks of the blend decrease in strength with increasing donor/acceptor ratio (Figure 6a). There is no big difference existing in UV−vis absorption spectra even for films of relatively favorable morphologies, such as that achieved in 1:2 blend ratio without or with 1% DIO (Figure 6b). Thus, other factors, such as charge separation and charge transport should be taken into account for the difference in J_{sc}.

Charge Carrier Transport. To make a realistic estimate of the charge carrier mobilities in the blend film and accurate comparison of electron and hole mobilities, we fabricated hole-only and electron-only devices with the same active layers as the PSCs. The electron and hole mobilities were then measured by fitting the dark $J-V$ curves for single carrier devices to space charge limited current (SCLC) model at low voltages, in which the current is given by $J = 9\varepsilon_0\varepsilon_r\mu V^2/8L^3\exp[0.891\gamma(V/L)^{0.5}]$,[40,41] where $\varepsilon_0\varepsilon_r$ represents the permittivity of the material, μ for the mobility, γ is the field activation factor, and L the thickness of the active layer. On the basis of the data from 9 devices for each condition, Figure 7 presents the statistically averaged hole and electron mobilities at different blend ratios. The hole mobility increases by about 2 orders of magnitude, from 3.25×10^{-6} to 1.44×10^{-4} cm^2 V^{-1} s^{-1}, while electron mobility fluctuates irregularly, a peak value shown at 1:2 blend ratio. Because of the nature of eutectic phase behavior and the effect of fullerene intercalation,[42,43] mobility change in blend films is closely related to the composition, size, and quality of separated phases formed. In 1:2 blend film, the eutectic phases with relatively larger size are estimated to comprise of both polymer chains and more intercalated fullerenes. The ordered arrangement of polymers and fullerenes in these eutectic phases helps to increase hole and

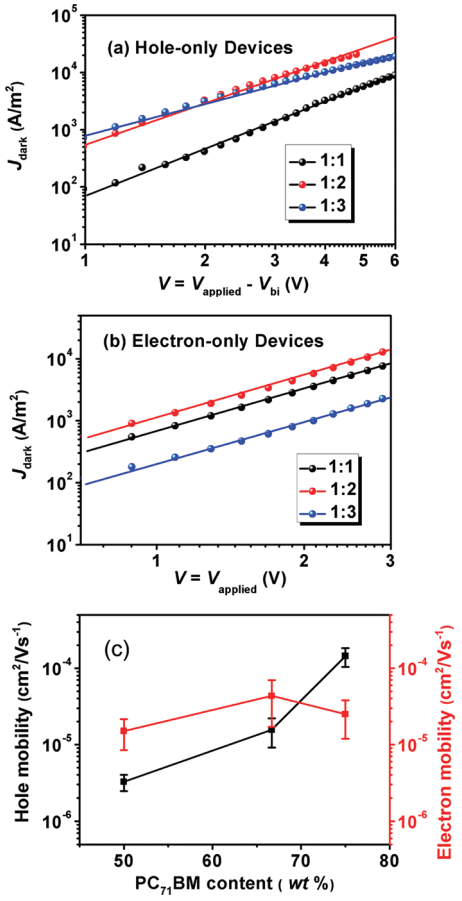

Figure 7. Measured $J-V$ characteristics under dark for (a) hole-only and (b) electron-only devices based on blend films with different blend ratios, and (c) variation tendency for hole and electron mobilities. The solid lines represent the fit to the experimental data using SCLC model. The bias is corrected for built-in potential (V_{bi}), arising from difference in the work function of the contacts, so that $V = V_{applied} - V_{bi}$. V_{bi} is 0.2 V. Error bars represent statistically calculated standard deviation for similar devices.

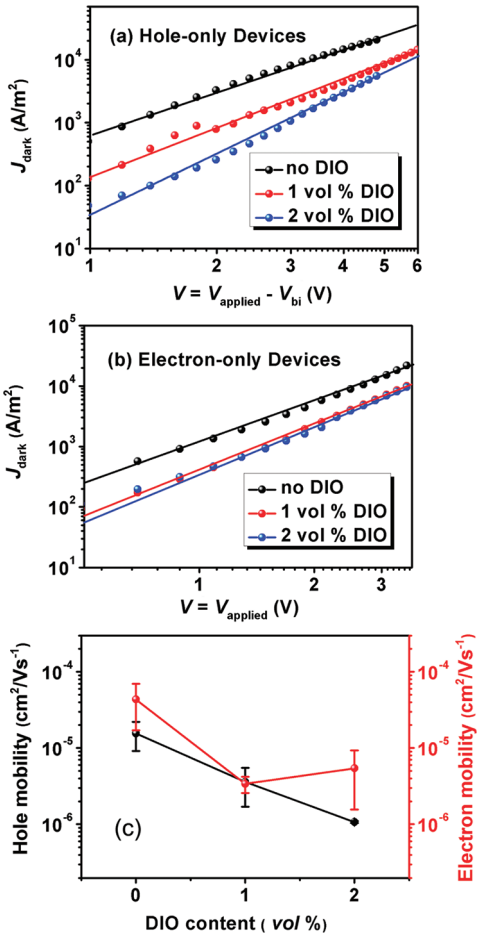

Figure 8. Measured $J-V$ characteristics under dark for (a) hole-only and (b) electron-only devices based on blend films formed with different additive content, and (c) variation tendency for hole and electron mobilities. The solid lines represent the fit to the experimental data using SCLC model. The bias is corrected for built-in potential (V_{bi}), arising from difference in the work function of the contacts, so that $V = V_{applied} - V_{bi}$. V_{bi} is 0.2 V. Error bars represent statistically calculated standard deviation for similar devices.

electron mobilities simultaneously. Thus, the gradual increase of hole mobility and the irregular fluctuation of electron mobility produce a balanced point at 1:2 blend ratio. This balanced charge transport is thought to be an important reason accounting for its higher J_{sc} and PCE.

The effect of additive content on charge carrier transport was also investigated, as shown in Figure 8. With DIO content increasing, hole and electron mobilities generally decrease. This should be attributed to the enhanced phase separation and the formation of larger eutectics, evidenced by the more distinct phase contrast (Figure 3) and larger aggregated domains (Figure 2) with DIO content increasing. The enhanced phase separation disfavors the connection of separated phases and thus reduces the hole and electron mobilities. A balanced point for electron and hole mobilities, close to 1:1, appears at 1 vol % DIO addition (Figure 8c). The balanced charge carrier transport may lower the charge accumulation at local interface and charge recombination, and facilitate collection of separated charge carriers. Thus, high J_{sc} and PCE can be obtained.

Loss Mechanism. To have an insight into the loss mechanism occurring in charge transport, the dependence of short-circuit current density (J_{sc}) on incident light power (ILP) was investigated.

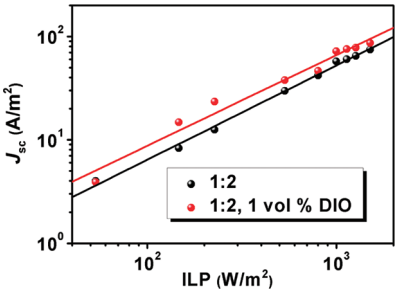

Figure 9. Measured short circuit current density (J_{sc}) versus incident light power (ILP) for two BHJ photovoltaic devices. The parameters S refer to the slope of J_{sc} vs ILP as $J_{sc} \sim \text{ILP}^S$. S is determined by a linear fit over the whole ILP range.

We plotted the logarithmic J_{sc}-ILP curves of two typical devices with 1:2 blend ratio or 1 vol % DIO additive, shown in Figure 9. The J_{sc} of both devices shows nearly linear dependence on ILP, giving slopes close to unity for the whole range of ICP ($J_{sc} = \text{ILP}^S$,

with $S \approx 1$), 0.91 and 0.88, respectively, suggesting the dominant role of geminate recombination rather than bimolecular recombination for both devices.[44] The geminate charge pair recombination (Onsager recombination) happens in BHJ thin films when charge separation distance is not sufficient to overcome the electrostatic attraction between electrons and holes.[45] This process significantly decreases the yield of long-lived and extractable charges in a way by transforming tightly bound charge pairs to ground state, excited singlet or triplet states in nanoseconds or hundreds of nanoseconds time scale. To reduce geminate recombination as possible, increased charge separation distance or large electron−hole pair separation probability would be beneficial. This can be achieved by enhancing internal electric field, increasing charge carrier transportation, or by decreasing mobility mismatch.[46,47] Both increased sum of electron and hole mobilities and balanced charge transport can increase the probability of charge-pair separation. However, the two typical devices, with 1:2 blend ratio or 1 vol % DIO additive, both of which exhibits relatively balanced charge transport, display an interesting phenomenon. The sum of electron and hole mobilities in the former is almost an order of magnitude higher than that of the latter. This generally means higher probability of charge-pair separation and higher performance, which obviously contradict with the actual result. This contradiction can not be explained solely by increased sum mobility and balanced charge transport. Other factors should also be involved, such as the phase separation morphology. As discussed in morphology section, 1 vol % DIO additive leads to moderate phase separation, which may help construct uniform and favorable internal electric field, while the formed polymer and/or $PC_{71}BM$ ordered phase can facilitate the charge transport and helps to reach a balance. For these reasons, large charge-pair separation probability and minimal geminate recombination can be expected. In conclusion, the highest J_{sc} achieved in this condition could be attributed to the generation of more long-lived and extractable charges via reducing geminate recombination. The reduced geminate recombination with gradually evolved morphology of improved phase separation and more balanced electron and hole mobilites is a factor that accounts for the improvement of device performance.

CONCLUSIONS

We have synthesized a new benzodithiophene-based polymer with good self-organization behavior and fabricated polymer/fullerene BHJ solar cells. By optimizing blend composition and additive content, evolved morphology with moderate nanoscale phase separation in PBDTBTZ:$PC_{71}BM$ blend film was achieved. The optimized morphology leads to the highest PCE ~3.2% of BHJ solar cells. The reason for performance enhancement is attributed to reduced geminate recombination loss due to evolved morphology and balanced charge carrier transport. The effect of evolved morphology on charge carrier transport in BHJ solar cells was probed, displaying a gradual balance tendency of hole and electron mobilities. Specially, the ratio of hole and electron mobilities close to the ideal value of 1:1 was achieved in the condition with 1:2 blend composition and 1 vol % 1, 8-diiodooctane addition.

AUTHOR INFORMATION

Corresponding Author

*E-mail: xwzhan@iccas.ac.cn; liyf@iccas.ac.cn.

ACKNOWLEDGMENT

Financial support by the NSFC (grants 21025418, 51011130028, 21021091, 20874106, 50933003), 973 Project (Grant 2011CB808401) and the Chinese Academy of Sciences is gratefully acknowledged.

REFERENCES

(1) Thompson, B. C.; Frechet, J. M. J. *Angew. Chem., Int. Ed.* **2008**, *47*, 58–77.
(2) Gunes, S.; Neugebauer, H.; Sariciftci, N. S. *Chem. Rev.* **2007**, *107*, 1324–1338.
(3) Li, Y. F.; Zou, Y. P. *Adv. Mater.* **2008**, *20*, 2952–2958.
(4) Park, S. H.; Roy, A.; Beaupre, S.; Cho, S.; Coates, N.; Moon, J. S.; Moses, D.; Leclerc, M.; Lee, K.; Heeger, A. J. *Nat. Photonics* **2009**, *3*, 297–303.
(5) Chen, H. Y.; Hou, J. H.; Zhang, S. Q.; Liang, Y. Y.; Yang, G. W.; Yang, Y.; Yu, L. P.; Wu, Y.; Li, G. *Nat. Photonics* **2009**, *3*, 649–653.
(6) Brabec, C. J.; Gowrisanker, S.; Halls, J. J. M.; Laird, D.; Jia, S. J.; Williams, S. P. *Adv. Mater.* **2010**, *22*, 3839–3856.
(7) Chen, J. W.; Cao, Y. *Acc. Chem. Res.* **2009**, *42*, 1709–1718.
(8) Cheng, Y. J.; Yang, S. H.; Hsu, C. S. *Chem. Rev.* **2009**, *109*, 5868–5963.
(9) Zhan, X. W.; Zhu, D. B. *Polym. Chem.* **2010**, *1*, 409–419.
(10) Blom, P. W. M.; Mihailetchi, V. D.; Koster, L. J. A.; Markov, D. E. *Adv. Mater.* **2007**, *19*, 1551–1566.
(11) Deibel, C.; Strobel, T.; Dyakonov, V. *Adv. Mater.* **2010**, *22*, 4097–4111.
(12) Peet, J.; Kim, J. Y.; Coates, N. E.; Ma, W. L.; Moses, D.; Heeger, A. J.; Bazan, G. C. *Nat. Mater.* **2007**, *6*, 497–500.
(13) Li, G.; Yao, Y.; Yang, H.; Shrotriya, V.; Yang, G.; Yang, Y. *Adv. Funct. Mater.* **2007**, *17*, 1636–1644.
(14) Reyes-Reyes, M.; Kim, K.; Carroll, D. L. *Appl. Phys. Lett.* **2005**, *87*, 083506.
(15) Zhang, F. L.; Jespersen, K. G.; Bjorstrom, C.; Svensson, M.; Andersson, M. R.; Sundstrom, V.; Magnusson, K.; Moons, E.; Yartsev, A.; Inganas, O. *Adv. Funct. Mater.* **2006**, *16*, 667–674.
(16) Ayzner, A. L.; Tassone, C. J.; Tolbert, S. H.; Schwartz, B. J. *J. Phys. Chem. C* **2009**, *113*, 20050–20060.
(17) Xin, H.; Ren, G. Q.; Kim, F. S.; Jenekhe, S. A. *Chem. Mater.* **2008**, *20*, 6199–6207.
(18) Girotto, C.; Moia, D.; Rand, B. P.; Heremans, P. *Adv. Funct. Mater.* **2011**, *21*, 64–72.
(19) Bavel, S.; Veenstra, S.; Loos, J. *Macromol. Rapid Commun.* **2010**, *31*, 1835–1845.
(20) Jo, J.; Na, S. I.; Kim, S. S.; Lee, T. W.; Chung, Y.; Kang, S. J.; Vak, D.; Kim, D. Y. *Adv. Funct. Mater.* **2009**, *19*, 2398–2406.
(21) Yu, G.; Gao, J.; Hummelen, J. C.; Wudl, F.; Heeger, A. J. *Science* **1995**, *270*, 1789–1791.
(22) Yang, X. N.; Loos, J.; Veenstra, S. C.; Verhees, W. J. H.; Wienk, M. M.; Kroon, J. M.; Michels, M. A. J.; Janssen, R. A. J. *Nano Lett.* **2005**, *5*, 579–583.
(23) van Bavel, S. S.; Sourty, E.; de With, G.; Loos, J. *Nano Lett.* **2009**, *9*, 507–513.
(24) Kim, J. S.; Park, Y.; Lee, D. Y.; Lee, J. H.; Park, J. H.; Kim, J. K.; Cho, K. *Adv. Funct. Mater.* **2010**, *20*, 540–545.
(25) Coakley, K. M.; McGehee, M. D. *Chem. Mater.* **2004**, *16*, 4533–4542.
(26) Mihailetchi, V. D.; van Duren, J. K. J.; Blom, P. W. M.; Hummelen, J. C.; Janssen, R. A. J.; Kroon, J. M.; Rispens, M. T.; Verhees, W. J. H.; Wienk, M. M. *Adv. Funct. Mater.* **2003**, *13*, 43–46.
(27) Peet, J.; Senatore, M. L.; Heeger, A. J.; Bazan, G. C. *Adv. Mater.* **2009**, *21*, 1521–1527.
(28) Woo, C. H.; Beaujuge, P. M.; Holcombe, T. W.; Lee, O. P.; Frechet, J. M. J. *J. Am. Chem. Soc.* **2010**, *132*, 15547–15549.
(29) Savenije, T. J.; Kroeze, J. E.; Yang, X. N.; Loos, J. *Adv. Funct. Mater.* **2005**, *15*, 1260–1266.

(30) Dante, M.; Yang, C.; Walker, B.; Wudl, F.; Nguyen, T. Q. *Adv. Mater.* **2010**, *22*, 1835–1839.
(31) Zhang, M. J.; Fan, H. J.; Guo, X.; He, Y. J.; Zhang, Z. G.; Min, J.; Zhang, J.; Zhao, G. J.; Zhan, X. W.; Li, Y. F. *Macromolecules* **2010**, *43*, 8714–8717.
(32) Hou, J. H.; Park, M. H.; Zhang, S. Q.; Yao, Y.; Chen, L. M.; Li, J. H.; Yang, Y. *Macromolecules* **2008**, *41*, 6012–6018.
(33) Liang, Y. Y.; Feng, D. Q.; Wu, Y.; Tsai, S. T.; Li, G.; Ray, C.; Yu, L. P. *J. Am. Chem. Soc.* **2009**, *131*, 7792–7799.
(34) Zhang, M. J.; Fan, H. J.; Cuo, X.; He, Y. J.; Zhang, Z. G.; Min, J.; Zhang, J.; Zhao, G. J.; Zhan, X. W.; Li, Y. F. *Macromolecules* **2010**, *43*, 5706–5712.
(35) Yuan, M. C.; Chiu, M. Y.; Liu, S. P.; Chen, C. M.; Wei, K. H. *Macromolecules* **2010**, *43*, 6936–6938.
(36) Li, G.; Shrotriya, V.; Huang, J. S.; Yao, Y.; Moriarty, T.; Emery, K.; Yang, Y. *Nat. Mater.* **2005**, *4*, 864–868.
(37) Li, G.; Shrotriya, V.; Yao, Y.; Yang, Y. *J. Appl. Phys.* **2005**, *98*, 043704.
(38) Lee, J. K.; Ma, W. L.; Brabec, C. J.; Yuen, J.; Moon, J. S.; Kim, J. Y.; Lee, K.; Bazan, G. C.; Heeger, A. J. *J. Am. Chem. Soc.* **2008**, *130*, 3619–3623.
(39) Erb, T.; Zhokhavets, U.; Gobsch, G.; Raleva, S.; Stühn, B.; Schilinsky, P.; Waldauf, C.; Brabec, C. J. *Adv. Funct. Mater.* **2005**, *15*, 1193–1196.
(40) Mihailetchi, V. D.; Xie, H.; Boer, B.; Koster, L. J. A.; Blom, P. W. M. *Adv. Funct. Mater.* **2006**, *16*, 699–708.
(41) Murgatroyd, P. N. *J. Phys. D: Appl. Phys.* **1970**, *3*, 151–156.
(42) Müller, C.; Ferenczi, T. A. M.; Campoy-Quiles, M.; Forst, J. M.; Bradley, D. D. C.; Smith, P.; Stingelin-Stutzmann, N.; Nelson, J. *Adv. Mater.* **2008**, *20*, 3510–3515.
(43) Mayer, A. C.; Toney, M. F.; Scully, S. R.; Rivnay, J.; Brabec, C. J.; Scharber, M.; Koppe, M.; Heeney, M.; McCulloch, I.; McGehee, M. D. *Adv. Funct. Mater.* **2009**, *19*, 1173–1179.
(44) Maturová, K.; van Bavel, S. S.; Wienk, M. M.; Janssen, R. A. J.; Kemerink, M. *Adv. Funct. Mater.* **2011**, *21*, 261–269.
(45) Pal, K. S.; Kesti, T.; Maiti, M.; Zhang, F.; Inganäs, O.; Hellström, S.; Andersson, R. M.; Oswald, F.; Langa, F.; Österman, T.; Pascher, T.; Yartsev, A.; Sundström, V. *J. Am. Chem. Soc.* **2010**, *132*, 12440–12451.
(46) Veldman, D.; İpek, Ö.; Meskers, C. J. S.; Sweelssen, J.; Koetse, M. M.; Veenstra, C. S.; Kroon, M. J.; Bavel, S. S.; Loos, J.; Janssen, A. J. R. *J. Am. Chem. Soc.* **2008**, *130*, 7721–7735.
(47) Wojcik, M.; Michalak, P.; Tachiya, M. *Appl. Phys. Lett.* **2010**, *96*, 162102.